RSC Advances

PAPER

View Article Online
View Journal | View Issue

Cite this: *RSC Adv.*, 2019, **9**, 42489

Sandwich-structure hydrogels implement on-demand release of multiple therapeutic drugs for infected wounds†

Tao Zheng,[a] Jinjian Huang,[ab] Yungang Jiang,[ab] Qinqing Tang,[a] Ye Liu,[ab] Ziyan Xu,[c] Xiuwen Wu*[a] and Jianan Ren *[a]

Wound infections bring huge challenges to clinical practice. A series of approaches are involved in the management of infected wounds including use of antibacterial agents, granulation tissue regeneration and scar prevention. In this study, we fabricated a sandwich-structure hydrogel dressing through layer-by-layer assembly of films and hydrogels. By pre-loading silver nanoparticles (AgNPs), vascular endothelial growth factors (VEGF) and ginsenoside Rg3 (Rg3) into each layer of the sandwich compound, this hydrogel could realize the sequential release of these drugs onto infected wound beds as demanded. Moreover, altering the thickness of middle layer could further change the drug delivery patterns characterized by delay at the initial releasing timepoint. When applying this dressing on infected wounds of rabbit ears, we found it could alleviate infection-induced inflammation, promote granulation tissue regeneration and inhibit scar formation. Collectively, the design of sandwich-structure hydrogels was facilitated to deliver specific drugs sequentially during their therapeutic time window for complicated diseases and has shown potential applications in infected wounds.

Received 12th November 2019
Accepted 4th December 2019

DOI: 10.1039/c9ra09412a

rsc.li/rsc-advances

1 Introduction

Hydrogels have outstanding advantages in delivering drugs because of their controlled delivery manner. Therapeutic drugs are loaded through simple mixture, linkage to one reactant or even direct participation in the formation of hydrogels.[1–3] Based on these methods, the drugs achieve sustained release or smart release regulated by outer stimuli such as pH, temperature, light, enzyme, ATP and electric field, *etc.*[4–9] The resulting different releasing patterns can adapt to the specific treatment requirements for abnormal cells or diseases. However, in most cases, rehabilitation can only be attained through multiple stages, during which specific drugs can be applied to reverse pathological process for each stage.

For this purpose, studies concerning the sequential release of two or more drugs are being carried out. For example, the hydrogel/microspheres system can deliver drugs at different times.[10,11] Such effects are also achieved using multilayer nanoparticles or microparticles and compartmental nanofibers.[12–15] These drug releasing systems share the similar principle that drugs loaded in the inner layer are released more slowly than those in the outer layer. In addition, the drugs themselves can affect releasing dynamics due to the differences of drug structure, hydrophilia and molecular weight,[16–18] which consequently lead to phased drug release. As a result, the drug releasing models can be regulated to meet multiple clinical demands.

Infected wounds are common but intractable healthcare issues, featured by the impairment of skin integrity and invasion of pathogens.[19,20] Patients with infected wounds suffer from pain, delayed discharge from hospital and financial loss. A satisfied treatment of infected wounds includes a series of approaches such as sufficient antisepsis, wound repair and anti-scar.[21,22] Targeting above three stages, we constructed a sandwich-structure hydrogel dressing that carried functional drugs in a film–hydrogel–film (FHF) architecture (Fig. 1). Silver nanoparticles (AgNPs) were loaded in basement film for antisepsis;[23] vascular endothelial growth factors (VEGF) were loaded in middle hydrogel for wound healing,[24] and ginsenoside Rg3 (Rg3) was loaded in top film for anti-scar. When applied on the infected wounds, the FHF structure enables these drugs to be released from top to down. We assume that the time drugs take to wound beds is different because of their spatial distributions, which may enable phased drug release consistent with wound healing process.

[a]*Laboratory for Trauma and Surgical Infections, Research Institute of General Surgery, Jinling Hospital, 305 East Zhongshan Road, Nanjing 210002, China. E-mail: lygwxw@163.com; jiananr@gmail.com*

[b]*School of Medicine, Southeast University, Nanjing 210009, China*

[c]*School of Medicine, Nanjing University, Nanjing 210093, China*

† Electronic supplementary information (ESI) available. See DOI: 10.1039/c9ra09412a

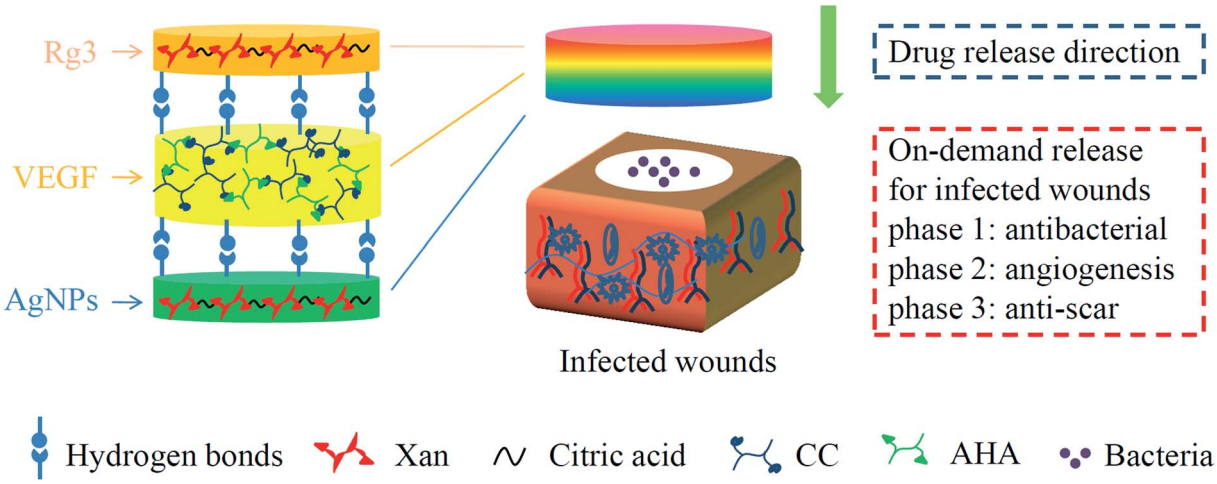

Fig. 1 Schematic diagram of sandwich-structure hydrogels through layer-by-layer assembly of films and hydrogels to realize the sequential release of AgNPs, VEGF and Rg3 onto wound beds for treatment. CC: carboxymethyl chitosan; AHA: aldehyde hyaluronic acid.

2 Materials and methods

2.1. Materials

Xanthan gum (xan, viscosity of 1% aqueous solution at 20 °C: 1450–2000 mPa s, TCI Development Co. Ltd, Shanghai, China); citric acid (Sigma-Aldrich, USA); hyaluronic acid sodium (HA, M_w: 2×10^5, HMC, China); chitosan (deacetylation degree: 85%, M_w: 2×10^5, Shanghai Aiyan Biotech Co. Ltd, China); sodium periodate (Sigma-Aldrich, USA); monochloroacetic acid (Sigma-Aldrich, USA); ethylene glycol (Sigma-Aldrich, USA); commercial AgNPs (size: ~60 nm, Shanghai Jianglai Co. Ltd); recombinant human vascular endothelial growth factor 121 (rhVEGF121, PeproTech Co. Ltd, USA); ginsenoside Rg3 (Rg3, purity > 98%, Nanjing Dilger Medical Technology Co. Ltd); all other reagents were of analytical reagent grade.

2.2. Synthesis of drug-loaded film–hydrogel–film dressing

2.2.1 Drug-loaded xan-based film. The generation of xan-based film was referred to the work by Bueno *et al.*[25] based on a crosslinking reaction (Fig. S1A†). Generally, 6 mg mL^{-1} of xan aqueous solution was mixed with citric acid at the concentration of 0.3 mg mL^{-1}. Then, the solution was poured onto a Teflon-coated plate and treated in a hot air oven at 50 °C until a film (thickness: ~0.2 mm) was casted. This casted film was peeled from the plate and treated in the oven again at 165 °C for 7 min. After cooling at room temperature, the film was stored in a sealed plastic bag at 4 °C. Based on the above procedures, the AgNP-loaded film was obtained by additional ultrasonic dispersion of AgNPs into xan aqueous solution at 40 μg mL^{-1},[23] and Rg3-loaded film was obtained by extra adding Rg3 methanol solution into xan aqueous solution at 220 μg mL^{-1}.

2.2.2 VEGF-loaded carboxymethyl chitosan (CC)/aldehyde hyaluronic acid (AHA) hydrogel. The CC/AHA hydrogel was synthesized based on Schiff base reaction (Fig. S2A†) in line with our previous work.[10] Generally, 5 g chitosan was suspended into 50 mL isopropyl alcohol. 25 mL of 10 mmol mL^{-1} NaOH solution was added dropwise and the resulting mixture was stirred for 30 min. Then, 50 mL of 60 wt% monochloroacetic acid solution was added and the entire mixed solution was heated with stirring at 60 °C for 3 h. After filtration and washing, the solid product (CC) was collected. AHA was obtained by oxidation of hyaluronic acid.[26] Briefly, 5 mL of 0.5 mmol mL^{-1} sodium periodate was added dropwise to 100 mL of 1 wt% hyaluronic acid aqueous solution, followed by stirring for 2 h at room temperature shielded from light. Then, the unreacted sodium periodate was neutralized by adding 1 mL ethylene glycol for 1 h. After dialysis and freeze drying, AHA was collected. The CC/AHA hydrogel was generated by equivolumetric mixture of CC and AHA at 24 mg mL^{-1} and 60 mg mL^{-1}, respectively. By premixing VEGF in CC solution at 0.5 μg mL^{-1}, the drug-loaded hydrogel was achieved.

2.2.3 Fabrication of drug-loaded sandwich-structure hydrogel dressing. The drug-loaded film was tailored in the same round shape with the cross section of syringe. We put AgNP-loaded film at the bottom, then injected VEGF-loaded hydrogel in the middle, and finally put Rg3-loaded film on the top. After complete gelation of CC and AHA (required time: ~60 s), the entire sandwich-structure hydrogel was extruded (Fig. S3†).

2.3. Characterization of sandwich-structure hydrogel dressing

2.3.1 FTIR spectrometry of xan-based film and CC/AHA hydrogel. The powders of xan, citric acid, xan-based film, chitosan, CC, hyaluronic acid, AHA and CC/AHA hydrogel were ground to a dry KBr disk and scanned at a resolution of 4 cm^{-1} in the wave number range of 4000–500 cm^{-1} using a Nicolet-6700 spectrometer (Thermo®, USA).

2.3.2 Swelling ratio of xan-based film and CC/AHA hydrogel. The hydrogel swelling ratio was determined by the following formula:[27]

$$\text{Swelling ratio} = (M_{\text{swollen gel}} - M_{\text{dried gel}})/M_{\text{dried gel}} \times 100\%;$$

$M_{\text{dried gel}}$ standed for the mass of dried hydrogel, and $M_{\text{swollen gel}}$ standed for the mass of swollen hydrogel at equilibrium.

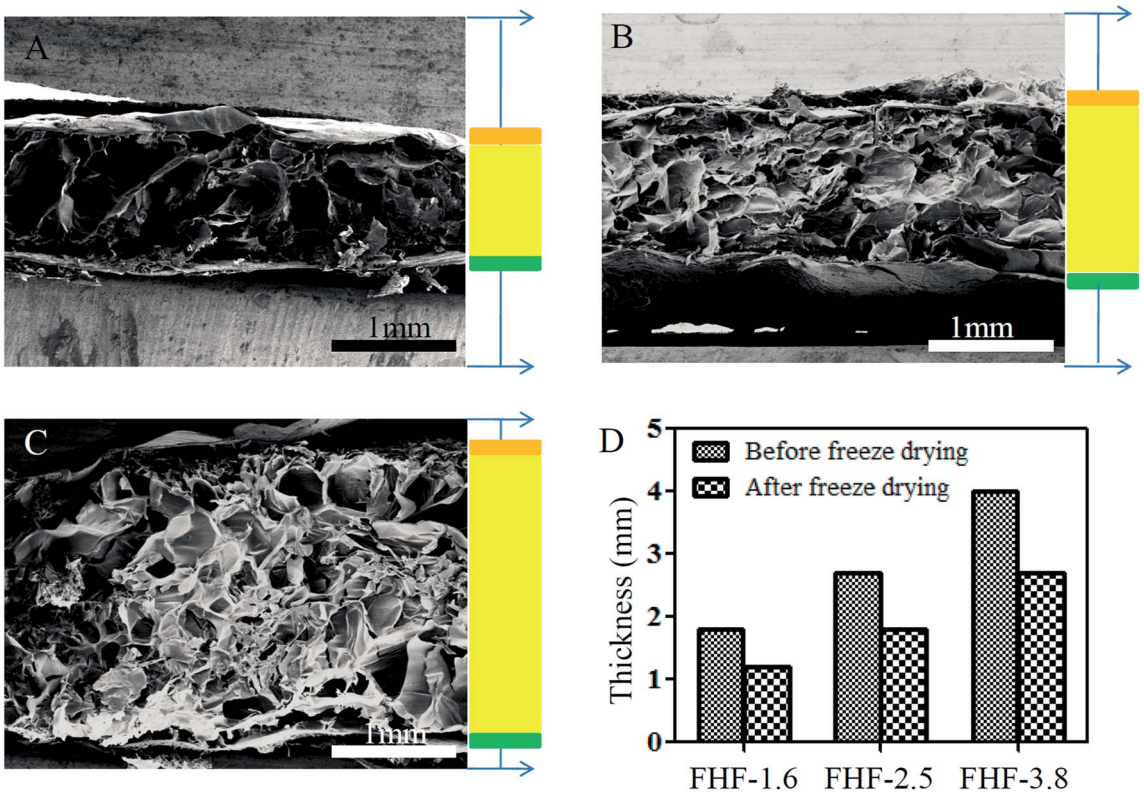

Fig. 2 Micromorphology of sand-structure hydrogels. (A) SEM image of FHF-1.6. (B) SEM image of FHF-2.5. (C) SEM image of FHF-3.8. (D) Thickness of sandwich-structure hydrogels before and after lyophilization. FHF-*x*: film–hydrogel–film assembled sandwich-structure dressing where its middle layer is *x* mm.

2.3.3 Morphology of sandwich-structure hydrogel dressing. The micromorphology of xan-based film and CC/AHA hydrogel was recorded by scanning electron microscopy (SEM). Briefly, the cross section of film and hydrogel was sprayed with gold and then observed under a scanning electron microscope (S-4800, Hitachi®, Japan).

2.4. Drug releasing assay

2.4.1 Test container. A modified syringe was used to carry the sandwich-structure hydrogel. This design enabled only AgNP-loaded film could contact with dispersion solution and almost imitated the real situation that only one surface of dressing could contact with wound bed.

2.4.2 Sample collection. After the sandwich-structure hydrogel was prepared in a modified syringe, we added 10 mL phosphate buffer solution (PBS, pH = 7.4) containing 0.5 wt% sodium dodecyl sulfate.[28] At each pre-defined interval time, 1 mL supernatant was retrieved and replaced with fresh dispersion solution.

2.4.3 Drug detection. AgNPs, VEGF and Rg3 in the collected supernatant were tested individually. The concentration of AgNPs was measured by an UV-visible spectrophotometry (METASH®, China) at the absorption peak of 400 nm. VEGF concentration was calculated using a VEGF ELISA assay kit (CUSABIO®, China). The amount of released Rg3 was determined by a high-performance liquid chromatography (HPLC, Thermo®, USA). The cumulative release was figured out from the ratio of above supplements in the supernatant to the total amount added in the sandwich-structure hydrogel.

2.5. Antibacterial assay *in vitro*

We prepared bacterial suspension of *S. aureus* and *E. coli* at the turbidity of 0.5 based on McFarland standards. Next, the bacterial suspensions were inoculated onto a mannitol salt agar plate (Bizheng Biotech Co. Ltd, China) followed by seeding drug-free hydrogel and drug loaded hydrogel on the plate surface. 24 h later, the bacteriostasis ring was recorded by a smart phone. Moreover, we incubated 10 mL 1 : 50 diluted bacterial suspension with drug-free hydrogel and drug-loaded hydrogel for 12 h at 37 °C. Then, the resulting bacterial suspensions were inoculated onto mannitol salt agar plates for 24 h, and images of bacterial colony formation were also recorded by a smart phone.

2.6. Cytocompatibility assay

The sandwich-structure hydrogels were placed in a 24-well plate and sterilized under ultraviolet light for 1 h. 1 mL of 1×10^4/mL fibroblasts were seeded on the surface of hydrogels. Live/dead staining was performed at 1 d and 3 d by adding 2 mM calcein AM and 4 mM ethidium homodimer to each well. After PBS washing, the images were recorded using a fluorescence

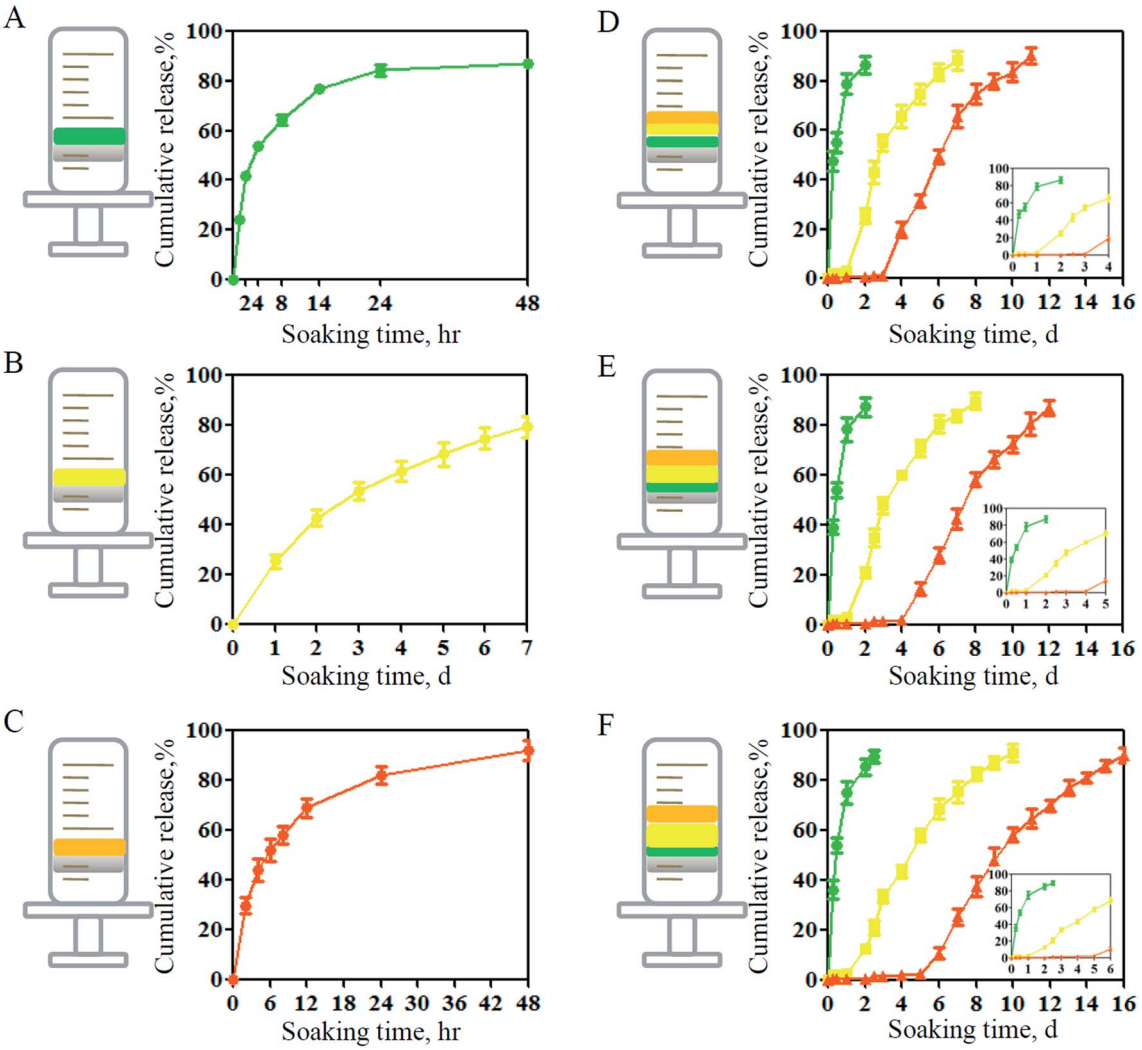

Fig. 3 *In vitro* drug releasing patterns detected by the one surface-contacted immersion method. (A) Simple AgNP-loaded film. (B) Simple VEGF-loaded hydrogel. (C) Simple Rg3-loaded film. (D) Drug-loaded FHF-1.6. (E) Drug-loaded FHF-2.5. (F) Drug-loaded FHF-3.8.

microscope. Cell viability was calculated according to the following formula:

$$\text{Cell viability} = N_{\text{green}}/(N_{\text{green}} + N_{\text{red}}) \times 100\%;$$

N_{green} represented the number of living cells (labeled in green) and N_{red} represented the number of dead cells (labeled in red). Three visual fields were randomly chosen to count cells. Moreover, we investigated the effect of leachate extracted from drug-loaded hydrogels on cell proliferation. 0.1 mL of 2×10^4/mL human umbilical vein endothelial cells (HUVECs) was added in wells (in triplicate) with 0.1 mL EMEM medium or 0.1 mL leachate. After incubation for 1 d, 2 d and 3 d, we added 20 μL of 5 mg mL^{-1} MTT reagent to each well. The resulting formazan salt was dissolved with 200 μL DMSO and then measured using a microplate spectrophotometer at 570 nm. The relative cell proliferation was calculated from the ratio of absorbance in leachate to that of EMEM medium.[29]

2.7. Acute infected wound models on rabbit ears

2.7.1 Animal preparation. Nine male New Zealand rabbits weighed around 2.5 kg were provided from Jinling Hospital. The rabbits were maintained at 25 °C under natural light–dark cycles and allowed free access to food and water. Propofol was used to carry out anesthesia through intravenous injection *via* ear vein. All the animal care and experimental protocols were performed in strict accordance with the chinese guideline for the care and use of laboratory animals (Ministry of Science and Technology [2006] file no. 398) and approved by Animal Investigation Ethics Committee of Jinling Hospital.

2.7.2 Experimental process. After anesthesia of rabbits, we removed two circular skins (~1 cm in diameter) for each ear. The four wounds of each rabbit were then treated by *S. aureus* + gauze, *S. aureus* + fibrin glue, fibrin glue, and *S. aureus* + drug-loaded sandwich-structure hydrogel, respectively. The wound healing process was recorded at 4 d, 9 d and 14 d. At each time point, three rabbits were sacrificed and their ear granulation

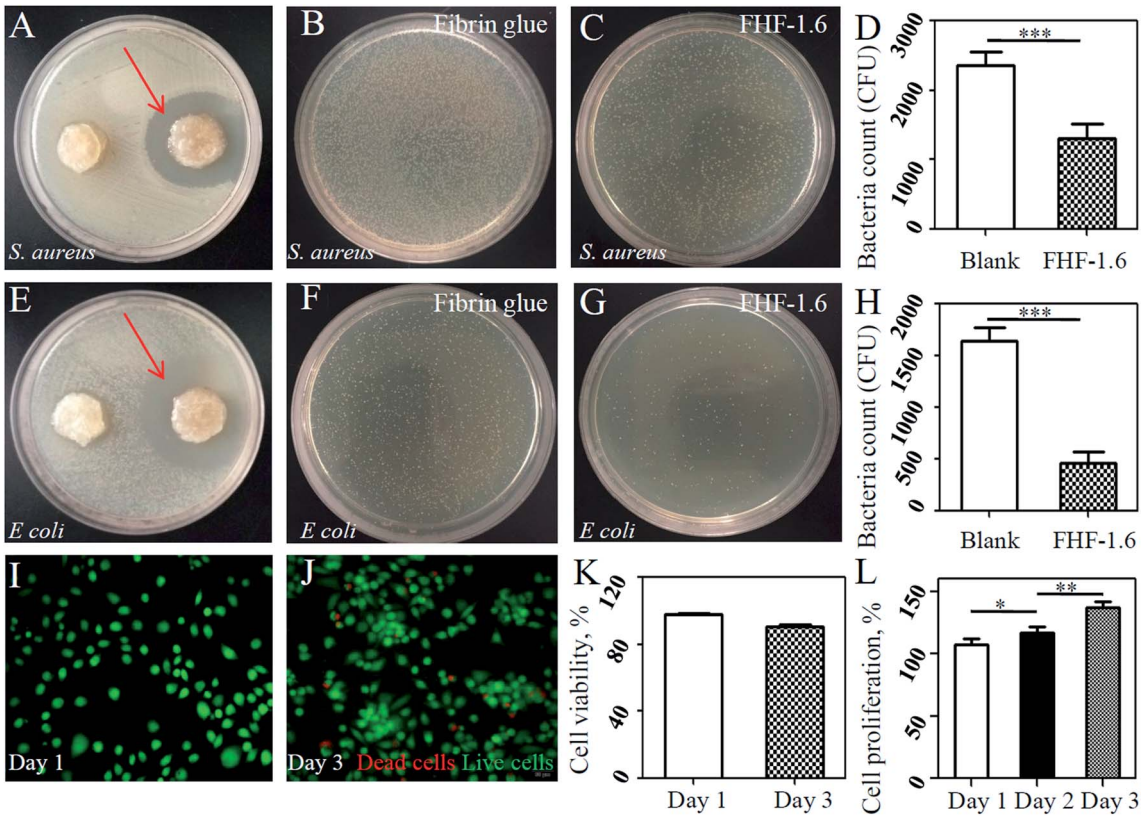

Fig. 4 *In vitro* antibacterial and biocompatible studies. (A) Inhibition zone of *S. aureus* generated by drug-loaded sandwich-structure hydrogels. Red arrows: inhibition zone. (B–D) Comparison of *S. aureus* colony formation by fibrin glue and drug-loaded sandwich-structure hydrogels, analyzed by Student's test. (E) Inhibition zone of *E. coli* generated by drug-loaded sandwich-structure hydrogels. Red arrows: inhibition zone. (F–H) Comparison of *E. coli* colony formation by fibrin glue and drug-loaded sandwich-structure hydrogels, analyzed by Student's test. (I–K) Live/dead staining of fibroblasts cultured on drug-loaded sandwich-structure hydrogels, analyzed by Student's test. (L) Cell proliferation of HUVECs cultured in leachate of drug-loaded sandwich-structure hydrogels compared to that in EMEM medium, analyzed by one-way ANOVA. *, $p < 0.05$; **, $p < 0.01$; ***, $p < 0.001$.

tissues were collected. The granulation thickness was evaluated by HE staining, and the inflammatory state was analyzed using mRNA transcription of inflammatory cytokines by qPCR (Table. S1†). CD31 and α-SMA fluorescent staining was used to identify vascularization. Furthermore, we evaluated the collagen deposition and fiber formation by Masson trichrome staining and western blot.

3 Results and discussion

3.1. Synthesis and characterization of sandwich-structure hydrogel

First, we applied the FTIR spectrometry to examine xan-based film. As shown in Fig. S1B,† xan had characteristic absorption bands at 1587 cm^{-1} and 1380 cm^{-1} due to the asymmetric and symmetric stretching vibrations of the COO^- groups. After heating the mixture of xan and citric acid, these two stretching vibrations were diminished, indicating the occurrence of crosslinking reaction between carboxy group of xan and hydroxy group of citric acid. Moreover, we analyzed the infrared spectrum of CC/AHA hydrogel (Fig. S2B†). Carboxylation of chitosan was verified because the stretching vibrations of the COO^- groups (1590 cm^{-1} and 1400 cm^{-1}) were increased, and we also confirmed aldehyde functionality of hyaluronic acid because the stretching vibrations at 1605 cm^{-1} and 1390 cm^{-1} were enlarged. The amino groups of CC and the aldehyde groups of AHA could crosslink with each other *via* a Schiff base reaction. The infrared spectrum of CC/AHA hydrogel was similar to that reported previously.[30,31]

Next, we fabricated a sandwich-structure hydrogel layer by layer through using xan-based film and CC/AHA hydrogel (Fig. S3†). The thickness of middle layer was tunable by altering the amount of CC/AHA hydrogel. In this study, we defined the middle layer as 1.6 mm, 2.5 mm and 3.8 mm in thickness. The SEM clearly revealed a film–hydrogel–film architecture and displayed the porous structure within each hydrogel (Fig. 2A–C). The surface between film and hydrogel was tightly contacted because of intermolecular hydrogen bond interactions. Notably, the entire thickness of sandwich-structure hydrogels was reduced when they were lyophilized (Fig. 2D), which indicated the dynamic restructuring of polymer networks during the loss of internal liquids.

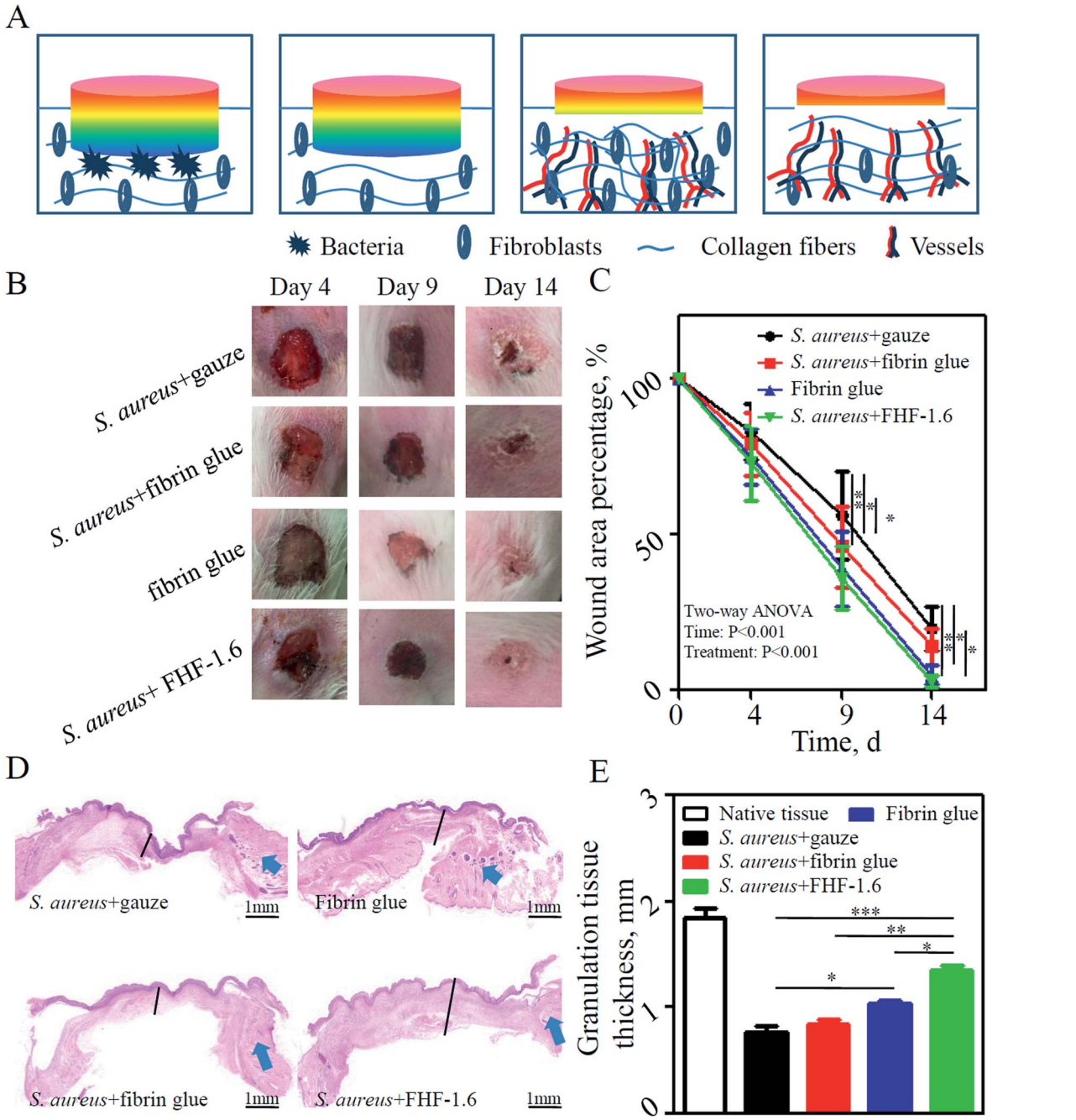

Fig. 5 Treatment effects of drug-loaded sandwich-structure hydrogels on infected wounds of rabbit ears. (A) Schematic diagram of recovery stages for infected wounds. (B) Images of infected wound healing treated by different interventions. (C) Comparison of wound area after using different interventions, analyzed by two-way ANOVA. (D) Comparison of granulation tissue regeneration in different groups by HE staining. (E) Thickness analysis of granulation tissues in different groups, analyzed by one-way ANOVA. *, $p < 0.05$; **, $p < 0.01$; ***, $p < 0.001$.

3.2. Drug releasing patterns of sandwich-structure hydrogel

In the traditional drug releasing assay, hydrogels are immersed in PBS and drugs can be released from the hydrogels in all directions.[32] However, for wound infection models, wound bed is the therapeutic site where the diffused drugs can take effects. Therefore, in this study, we conducted the drug releasing assay using a specific test container. This container enabled that only one surface was in contact with PBS. By this method, we firstly detected the drug release in each separate layer. As shown in Fig. 3A–C, both film and hydrogel could release internal drugs in a controlled manner, and the releasing duration of VEGF was longer than that of AgNPs and Rg3. The possible reason could be that there was smaller specific surface area of hydrogels than that of films and larger molecular weight of VEGF than that of the other two drugs.[18] When fabricating the compounds layer-by-layer, we could observe that there was a delay of initial release for VEGF and Rg3 due to the barrier effects (Fig. 3D). More

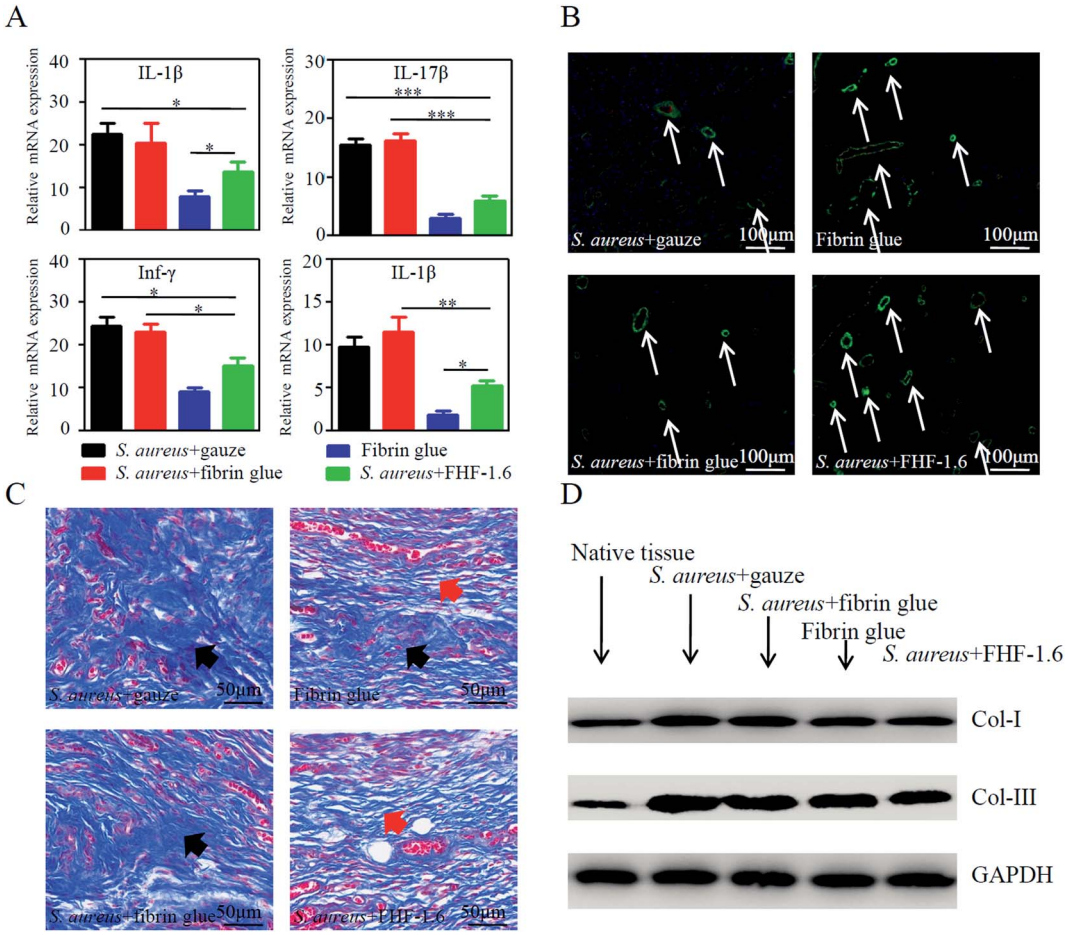

Fig. 6 Analysis of inflammation, vessel formation and collagen fiber deposition of granulation tissues at different stages. (A) Relative mRNA expression of proinflammatory cytokines in granulation tissues treated by different interventions at day 4, analyzed by one-way ANOVA. (B) Immunofluorescent staining of vessels in granulation tissues after using different treatments at day 9. CD31: red staining; α-SMA: green staining; (C) Masson trichrome staining of collagen fibers in granulation tissues of different groups at day 14. Black arrows: inordinate fibers; red arrows: well-organized fibers. (D) Semiquantitative analysis of collagen fibers by western blot in granulation tissues of different groups at day 14. *, $p < 0.05$; **, $p < 0.01$; ***, $p < 0.001$.

interestingly, the initial releasing time was further postponed if the thickness of hydrogel was increased (Fig. 3E and F). The above results indicated that the sandwich-structure hydrogels could realize the adjustable sequential release of drugs as demanded, therefore having great potentials as wound dressings.

3.3. Antibacterial property of sandwich-structure hydrogel

Next, we evaluated the antibacterial ability of the sandwich-structure hydrogel. After loading with drugs, this hydrogel could exhibited antiseptic effects to *S. aureus* and *E. coli* confirmed by the appearance of bacteriostasis ring (Fig. 4A and E) and the reduction of bacterial colony formation (Fig. 4B–D and F–H). This was attributed to the presence of AgNPs, which could kill bacteria by collapsing bacterial membrane and prohibiting DNA unwinding.[33] To our knowledge, persistent wound infection is the main reason leading to wound chronicity characterized by the formation of bacterial biofilm. Macrophages and other immune cells can not physically reach bacteria to engulf them since they are trapped within the biofilm architecture, consequently causing cell death and inflammation enlargement.[34] To remove this core factor, in this study, we loaded AgNPs in the bottom layer to achieve the antibacterial purpose at the very early stage. Therefore, this design was reasonable from clinical aspects.

3.4. Biocompatibility of sandwich-structure hydrogel

We further evaluated biosafety of the hydrogel dressing as it is always an important consideration for translational medicine. In this study, it was found that fibroblasts demonstrated high rates of cell viability after cultured on hydrogel surface (Fig. 4I–K). Moreover, the HUVECs had a higher proliferation rate when cultured in leachate of drug-loaded hydrogels than that of drug-free hydrogels. It suggested that VEGF maintained its biological activities and the potential cytotoxity risk of released AgNPs could be neglected.[35]

3.5. Promotion of wound healing by sandwich-structure hydrogel

As shown in Fig. 5A, the stages for recovery of infected wound included antibacteria, vessel and fiber regeneration, and fiber

reconstruction. In our experiments, we found that the sandwich-structure hydrogel could promote the infected wound healing of rabbit ears compared with other infected groups (Fig. 5B and C). At day 9 postoperatively, the granulation tissues were harvested and their average thickness was higher in the sandwich-structure hydrogel group than that in other groups (Fig. 5D and E). This was possibly due to the potent angiogenesis competence of VEGF. To further confirm it, we stained the vessels in granulation tissues using CD31 and α-SMA, which were biomarkers of vascular endothelial cells and capillary formation, respectively. The results indicated that the application of sandwich-structure hydrogels could promote vessel formation (Fig. 6B and S4A†). Moreover, the inflammatory state of granulation tissues at day 4 was detected using qPCR. It was found that the transcription levels of proinflammatory factors were reduced in the sandwich-structure hydrogel group compared with those of other infected groups (Fig. 6A). However, in contrast to the non-infected fibrin glue group, the proinflammatory levels of sandwich-structure hydrogel group were relatively higher possibly due to that the bacterial debris could generate inflammation through pathogen-associated molecular patterns.[36,37] At last, we evaluated the fiber deposition of granulation tissues. Excessive fiber deposition is a risk factor of hypertrophic scar formation. From the Masson trichrome staining (Fig. 6C), it was found that abundant and inordinate fibers were deposited in the infected gauze group and fibrin glue group at day 14, while fibers in the non-infected fibrin glue group and infected sandwich-structure hydrogel group were relatively sparse and organized. The results of western blot also indicated that the quantity of fibers in the sandwich-structure hydrogel group was smaller (Fig. 6D, S4B and S4C†). Together, this animal study demonstrated that drug-loaded sandwich-structure hydrogels could alleviate the pathogen-induced inflammation, promote the neovascular formation and reduce the fiber deposition for each stage of wound healing.

4 Conclusion

In this study, we produced a sandwich-structure hydrogel dressing through layer-by-layer fabrication of film, hydrogel and film. By pre-loading specific drugs into each layer, this dressing could realize the sequential release of drugs onto wound beds on demands of antibacteria, vessel regeneration and fiber inhibition. This design showed the great potentials of hydrogel assemblies at the macro level in drug delivery, and they might have wide applications in the treatment of complicated diseases including infected wounds.

Author contributions

Tao Zheng, Xiuwen Wu and Jianan Ren conceived and designed the experiments; Tao Zheng, Jinjian Huang, Yungang Jiang, Ye Liu, Ziyan Xu performed the experiments; Tao Zheng and Qinqing Tang analyzed the data; Xiuwen Wu and Jianan Ren contributed reagents/materials/analysis tools; Tao Zheng and Jinjian Huang wrote the paper.

Conflicts of interest

We declare no potential conflicts of interest concerning the research, authorship, and/or publication of this article.

Acknowledgements

We thank Tingting Xu in Nanjing Tech University for instructions regarding the high-performance liquid chromatography. The study was supported by General Project of Military Logistics Research (CLB19J025), Key Project of Science Foundation of the 12th Five-Year Plan (BNJ13J002), Innovation Project of Military Medicine (16CXZ007), Distinguished Scholars Foundation of Jiangsu Province (JCRCB2016006), Key Project of Jiangsu Social Development (BE2017722), Nanjing Science and Technology Development Project (201803051), China Jiangsu Planned Projects for Postdoctoral Research Funds (2019K283) and China Postdoctoral Science Foundation (2016M602982).

References

1 M. Hamidi, A. Azadi and P. Rafiei, *Adv. Drug Delivery Rev.*, 2008, **60**, 1638–1649.
2 J. Hu, Y. Quan, Y. Lai, Z. Zheng, Z. Hu, X. Wang, T. Dai, Q. Zhang and Y. Cheng, *J. Controlled Release*, 2017, **247**, 145–152.
3 J. Huang, Y. Ren, X. Wu, Z. Li and J. Ren, *J. Tissue Eng.*, 2019, **10**, 1013333264.
4 D. Lyu, S. Chen and W. Guo, *Small*, 2018, **14**, e1704039.
5 D. Aycan and N. Alemdar, *Carbohydr. Polym.*, 2018, **184**, 401–407.
6 S. Mongkolkitikul, N. Paradee and A. Sirivat, *Eur. J. Pharm. Sci.*, 2018, **112**, 20–27.
7 W. C. Liao, S. Lilienthal, J. S. Kahn, M. Riutin, Y. S. Sohn, R. Nechushtai and I. Willner, *Chem. Sci.*, 2017, **8**, 3362–3373.
8 H. Shang, X. Chen, Y. Liu, L. Yu, J. Li and J. Ding, *Int. J. Pharm.*, 2017, **527**, 52–60.
9 S. W. Lv, Y. Liu, M. Xie, J. Wang, X. W. Yan, Z. Li, W. G. Dong and W. H. Huang, *ACS Nano*, 2016, **10**, 6201–6210.
10 J. Huang, J. Ren, G. Chen, Z. Li, Y. Liu, G. Wang and X. Wu, *Mater. Sci. Eng., C*, 2018, **89**, 213–222.
11 X. Kong, W. Xu, C. Zhang and W. Kong, *Exp. Ther. Med.*, 2018, **15**, 1442–1448.
12 A. Jimenez, R. A. Bilbeisi, T. K. Ronson, S. Zarra, C. Woodhead and J. R. Nitschke, *Angew. Chem., Int. Ed. Engl.*, 2014, **53**, 4556–4560.
13 B. J. Zhang, Z. W. Han, K. Duan, Y. D. Mu and J. Weng, *J. Biomed. Mater. Res.*, 2018, **106**, 95–105.
14 X. Luo, H. Zhang, M. Chen, J. Wei, Y. Zhang and X. Li, *Int. J. Pharm.*, 2014, **475**, 438–449.
15 J. Meng, V. Agrahari, M. J. Ezoulin, S. S. Purohit, T. Zhang, A. Molteni, D. Dim, N. A. Oyler and B. C. Youan, *AAPS J.*, 2017, **19**, 692–702.
16 A. J. Rufaihah, N. A. Johari, S. R. Vaibavi, M. Plotkin, D. T. Di Thien, T. Kofidis and D. Seliktar, *Acta Biomater.*, 2017, **48**, 58–67.

17 R. Lopez-Cebral, G. Peng, L. L. Reys, S. S. Silva, J. M. Oliveira, J. Chen, T. H. Silva and R. L. Reis, *J. Mater. Sci.: Mater. Med.*, 2018, **29**, 21.
18 B. J. Peret and W. L. Murphy, *Adv. Funct. Mater.*, 2008, **18**, 3410–3417.
19 M. Malone, K. Johani, S. O. Jensen, I. B. Gosbell, H. G. Dickson, H. Hu and K. Vickery, *EBioMedicine*, 2017, **21**, 142–149.
20 C. B. Creech, D. N. Al-Zubeidi and S. A. Fritz, *Infect. Dis. Clin. North Am.*, 2015, **29**, 429–464.
21 E. Davies and M. King, *J. Clin. Aesthet. Dermatol.*, 2017, **10**, E5–E7.
22 X. Chen, L. H. Peng, Y. H. Shan, N. Li, W. Wei, L. Yu, Q. M. Li, W. Q. Liang and J. Q. Gao, *Int. J. Pharm.*, 2013, **447**, 171–181.
23 J. Huang, J. Ren, G. Chen, Y. Deng, G. Wang and X. Wu, *J. Nanomater.*, 2017, **2017**, 1–10.
24 J. Huang, Y. Deng, J. Ren, G. Chen, G. Wang, F. Wang and X. Wu, *Carbohydr. Polym.*, 2018, **186**, 54–63.
25 V. B. Bueno, R. Bentini, L. H. Catalani and D. F. Petri, *Carbohydr. Polym.*, 2013, **92**, 1091–1099.
26 S. Khunmanee, Y. Jeong and H. Park, *J. Tissue Eng.*, 2017, **8**, 1545511424.
27 J. Huang, Z. Li, Q. Hu, G. Chen, Y. Ren, X. Wu and J. Ren, *iScience*, 2018, **8**, 40–48.
28 T. Xu, R. Yang, X. Ma, W. Chen, S. Liu, X. Liu, X. Cai, H. Xu and B. Chi, *Adv. Healthcare Mater.*, 2019, **8**, e1900123.
29 J. J. Huang, J. A. Ren, G. F. Wang, Z. A. Li, X. W. Wu, H. J. Ren and S. Liu, *World J. Gastroenterol.*, 2017, **23**, 7489–7494.
30 L. Li, N. Wang, X. Jin, R. Deng, S. Nie, L. Sun, Q. Wu, Y. Wei and C. Gong, *Biomaterials*, 2014, **35**, 3903–3917.
31 Y. Deng, J. Ren, G. Chen, G. Li, X. Wu, G. Wang, G. Gu and J. Li, *Sci. Rep.*, 2017, **7**, 2699.
32 L. Huang, H. Zhang, S. Wu, X. Xu, L. Zhang, H. Ji, L. He, Y. Qian, Z. Wang, Y. Chen, J. Shen, Z. W. Mao and Z. Huang, *iScience*, 2019, **19**, 224–231.
33 K. I. Batarseh, *J. Antimicrob. Chemother.*, 2004, **54**, 546–548.
34 C. R. Arciola, D. Campoccia, P. Speziale, L. Montanaro and J. W. Costerton, *Biomaterials*, 2012, **33**, 5967–5982.
35 J. Wongpreecha, D. Polpanich, T. Suteewong, C. Kaewsaneha and P. Tangboriboonrat, *Carbohydr. Polym.*, 2018, **199**, 641–648.
36 K. P. Acker, F. L. T. Wong, E. West, J. Craft, A. Narechania, H. Smith, K. O'Brien, A. M. Moustafa, C. Lauren, P. J. Planet and A. Prince, *iScience*, 2019, **19**, 281–290.
37 S. S. Ben, O. Mouhadeb, K. Cohen, C. Varol and N. Gluck, *iScience*, 2019, **14**, 147–163.